The Link between Submillimetre Galaxies and Luminous Ellipticals: Near-Infrared IFU Spectroscopy of Submillimetre Galaxies

A. M. Swinbank,[1]* S. C. Chapman,[2] Ian Smail,[1] C. Lindner,[2] C. Borys,[2,3] A. W. Blain,[2] R. J. Ivison,[4,5] & G. F. Lewis[6]

[1] *Institute for Computational Cosmology, Department of Physics, Durham University, South Road, Durham, DH1 3LE, UK*
[2] *Astronomy Department, California Institute of Technology, 105-24, Pasadena, CA 91125, USA*
[3] *University of Toronto, Toronto, Ontario, Canada M5S 3H8, Canada*
[4] *Astronomy Technology Center, Royal Observatory, Blackford Hill, Edinburgh, EH19 3HJ, UK*
[5] *Institute for Astronomy, University of Edinburgh, Edinburgh, EH19 3HJ, UK*
[6] *School of Physics, University of Sydney, NSW 2006, Australia*
* *Email: a.m.swinbank@durham.ac.uk*

5 February 2008

ABSTRACT

We present two-dimensional spectroscopy covering the rest-frame wavelengths of strong optical emission lines in six luminous submillimetre galaxies at $z = 1.3$–2.5. Using this near-infrared integral field spectroscopy together with *Hubble Space Telescope* ACS and NICMOS imaging we map the dynamics and morphologies of these systems on scales from 4–11 kpc. Four of the systems show multiple components in their spatially-resolved spectra with average velocity offsets of $\sim 180 \, \mathrm{km \, s^{-1}}$ across 8 kpc in projection. From the ensemble properties of eight galaxies, from our survey and the literature, we estimate the typical dynamical masses of bright submillimetre galaxies as $5 \pm 3 \times 10^{11} \, \mathrm{M_\odot}$. This is similar to recent estimates of their stellar masses – suggesting that the dynamics of the central regions of these galaxies are baryon dominated, with a substantial fraction of those baryons in stars by the epoch of observation. Combining our dynamical mass estimates with stellar luminosities for this population we investigate whether submillimetre galaxies can evolve onto the Faber-Jackson relation for local ellipticals. Adopting a typical lifetime of $\tau_{\mathrm{burst}} \sim 300 \, \mathrm{Myr}$ for the submillimetre-luminous phase – using the latest estimates of gas masses, star formation rates and AGN contribution to the bolometric luminosities – we find that the stellar populations of submillimetre galaxies should fade to place them on the Faber-Jackson relation, at $\mathrm{M}_K \sim -25.1$. Furthermore, using the same starburst lifetime we correct the observed space density of submillimetre galaxies for the duty cycle to derive a volume density of the progenitors of $\sim 1 \times 10^{-4} \, \mathrm{Mpc^{-3}}$. This is consistent with the space density of local luminous early-type galaxies with $\mathrm{M}_K \sim -25.1$, indicating that submillimetre galaxies can evolve onto the scaling relations observed for local early-type galaxies, and the observed population at $z \sim 2$ is then sufficient to account for the formation of the whole population of $\gtrsim 3L_K^*$ ellipticals seen at $z \sim 0$.

Key words: galaxies: high-redshift, submillimetre; — galaxies: evolution; — galaxies: star formation rates, AGN; — galaxies: individual

1 INTRODUCTION

Deep optical and near-infrared imaging with the superlative resolution of the NICMOS and ACS cameras onboard *Hubble Space Telescope* (*HST*) has made it possible to study the morphologies and colours of high-redshift far-infrared luminous galaxies identified in the sub-millimetre (submm) waveband in unprecedented levels of detail (Smail et al. 1998, 2002; Chapman et al. 2003b; Smail et al. 2004; Pope et al. 2005; Almaini et al. 2005). By combining this data with spectroscopically confirmed redshifts (Chapman et al. 2003a, 2005), we are beginning to understand the processes which triggers the immense bolo-

metric luminosity output in these galaxies, allowing us to address issues such as their true contribution to the star-formation rate history of the Universe (e.g., Chapman et al. 2005). Submm galaxies (SMGs) are amongst the most bolometrically luminous galaxies in the Universe (with $L_{\rm bol} \sim 10^{13}$ L$_\odot$ and a median redshift of $< z > \sim 2.2$). However, in contrast to quasars at the same early epochs, their bolometric output appears to be dominated by star-formation rather than AGN activity (Swinbank et al. 2004; Alexander et al. 2005). It is clearly important to establish firmly the masses for these galaxies in order to understanding the rapid evolution of the submm population. Such diagnostics will allow us to determine how they relate to present-day galaxies and in particular to test whether they represent the formation phase of the most massive elliptical galaxies at the present-day, as many suspect (Lilly et al. 1999).

To probe the dynamical structures of these frequently complex systems requires a reliable separation of the spatial and spectral information. One particularly powerful approach to achieve this is using millimetric CO emission line maps to trace the distribution and kinematics of dense gas within the galaxies (Frayer et al. 1999, 2003; Neri et al. 2003; Greve et al. 2005) especially at high resolution (Genzel et al. 2003; Downes & Solomon 2003; Tacconi et al. 2006). Unfortunately, prior to the commissioning of the Atacama Large Millimetre Array, this approach remains observationally very demanding, typically requiring 30 hours per source with the IRAM interferometer and can only be applied to the most massive and gas-rich SMGs. An alternative tool which is less demanding in terms of telescope time and can provide spatially-resolved dynamics of SMGs with sufficient spatial and velocity resolution to study their internal structure is near-infrared integral field spectroscopy targeting the rest-frame optical emission lines such as [O III]λ5007 and H$\alpha\lambda$6563 (e.g. Tecza et al. 2004; Swinbank et al. 2005). The spectroscopic maps so produced allow us trace the dynamical and structural properties of SMGs on scales of a few kpc, pin-point the sites of active star formation and identify non-thermal emission from active galactic nuclei (AGN) in components within these systems. However, they are also subject to potential biases due to extreme extinction within some regions of the SMGs and from outflows in the emission-line gas which is being observed (Bower et al. 2004; Wilman et al. 2005). While the star formation rates estimated from the Hα are typically a factor of 10–100 $\times$ less than that predicted from the far-infrared emission (suggesting to 1–4 magnitudes of dust absorption; q.v. Smail et al. 2004), it is clear that the Hα emission provides a more secure probe of the star-formation rates and dynamics than either the Lyα emission or rest-frame UV continuum and can thus provide a reliable and observationally efficient probe of the activity and dynamics of this important population.

Using the UIST near-infrared Integral Field Unit (IFU) at UKIRT and the GNIRS IFU at Gemini-South we have studied the rest-frame optical emission line properties of six submillimetre galaxies at $z = 1.3$–2.5. These observations, together with high-resolution imaging from *HST* allow us to probe the physical cause of the rapid evolution of submillimetre galaxies, enabling us to test whether these far-infrared luminous galaxies comprise merging systems which are likely to be the progenitors of local massive ellipticals, or

whether instead they are simply high-luminosity episodes in the history of more mundane galaxies. Our paper is laid out as follows: in §2 we present the observations and their reduction. In §3 we discuss the analysis of these data, while in §4 and §5 we present our discussion and conclusions respectively. We use a cosmology with $H_0 = 70\,{\rm km\,s^{-1}}$, $\Omega_M = 0.3$ and $\Omega_\Lambda = 0.7$ in which $1''$ corresponds to 8.2 kpc at $z = 2.5$ and 8.5 kpc at $z = 1.5$.

2   OBSERVATIONS AND REDUCTION

The SMGs in this paper come from surveys at 850 or 1200μm by Scott et al. (2002); Greve et al. (2004) and Webb et al. (2003b). These sources were spectroscopically identified by Chapman et al. (2003a, 2005) and confirmed with precise redshifts from Swinbank et al. (2004) based on accurate radio positions (e.g. Ivison et al. 2002). We also include the recently discovered hyper-luminous far-infrared-selected galaxy MIPS J142824.0+352619 from Borys et al. (2006) aswell as an optically faint radio galaxy (OFRG) which was tentatively detected as a millimeter continuum source in Greve et al. (2005) for which a spectroscopic redshift was measured by Chapman et al. (2006). The coordinates and redshifts for each source are reported in Table 1 and we briefly review the properties of each individual source here.

2.1   Sample

CFRS 03.15: First identified in the Canada-UK Deep Submm Survey by Webb et al. (2003a), this submm galaxy has $S_{850} = 4.4 \pm 1.1$ mJy and a 1.4GHz flux density of $S_{1.4\rm GHz} = 226 \pm 12\mu$Jy. Spectroscopic observations from Chapman et al. (2005) and Swinbank et al. (2004) yield a redshift of $z = 1.4076$ which implies a luminosity of $L_{FIR} = 5.8 \pm 1.5 \times 10^{12}$ L$_\odot$. The rest-frame UV spectroscopy from Chapman et al. (2005) shows strong C IV emission, which along with the high [N II]/Hα line ratio and apparent underlying broad Hα line in the near-infrared spectra from Swinbank et al. (2004) suggests substantial AGN activity.

N2 850.7: This submm-selected galaxy has $S_{850} = 9.0 \pm 2.4$ mJy, lies at $z = 1.488$, and has a far-infrared luminosity of $L_{\rm FIR} = 6.4 \pm 1.7 \times 10^{12}$ L$_\odot$ (Chapman et al. 2005). The existing optical and near-infrared spectroscopy of this source suggest that the bolometric luminosity is predominantly arising from a star-burst, with low [N II]/Hα and C IV/Lyα emission line ratios (Chapman et al. 2005; Swinbank et al. 2004). Interferometric observations of the molecular CO emission in this system by Greve et al. (2005) failed to detect the CO(2-1) line. If the gas reservoir within this galaxy is close to the systemic redshift, indicated by the Hα emission line, then this non-detection implies an upper limit of $< 1.8 \times 10^{10}$ M$_\odot$ on the H$_2$ gas mass.

N2 1200.18: The near-infrared spectroscopy of N2 1200.18 indicates a redshift of $z = 2.592$ (Swinbank et al. 2004), and its 1200μm flux density of $2.2 \pm 0.6\,\mu$Jy then corresponds to a far-infrared luminosity of $L_{\rm FIR} = 10.9 \pm 3.0 \times 10^{12}$ L$_\odot$ for a reasonable template SED. The radio flux density ($S_{1.4\rm GHz} = 180 \pm 22\mu$Jy) is relatively strong, suggesting a possible contribution from an AGN. This is confirmed by the existing longslit optical and near-infrared spectroscopy which shows high
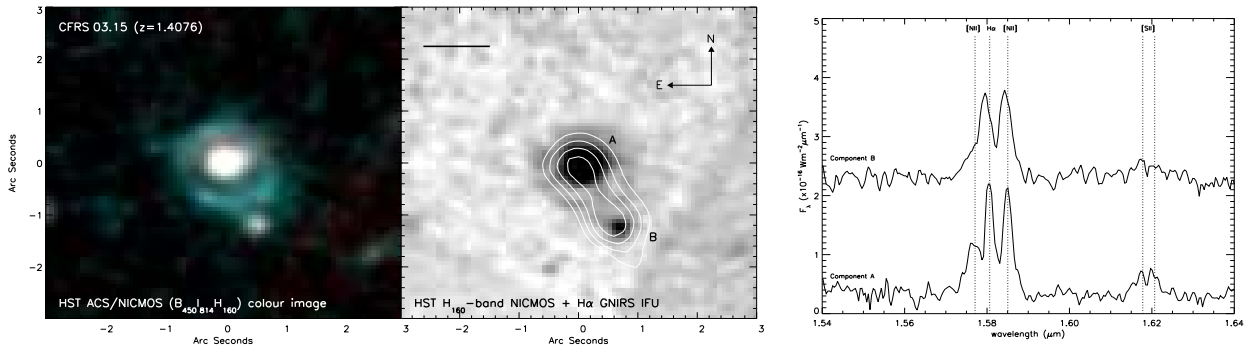
Figure 1. *Left:* True colour *HST* ACS/NICMOS $B_{450} I_{814} H_{160}$-band image of CFRS 03.15 at $z=1.4076$ showing the complex morphology (the colour image is displayed in log scale to emphasise the morphology). *Middle:* *HST* NICMOS H_{160}-band image of CFRS 03.15 with the Hα emission line map from the GNIRS IFU observations overlaid as contours, showing that the bright knot located $\sim 1.3''$ (~ 11 kpc) to the South-West is associated with the system. The solid bar represents the FWHM of the seeing disk for the IFU observations. *Right:* Spectra from the two components seen in the *HST* imaging of CFRS 03.15 from the Keck/NIRSPEC observation. The top spectrum is offset in flux for clarity. From our spectroscopy, the compact component to the South-West is blue-shifted by 90 ± 20 km s^{-1} in projection from the nucleus, suggesting they are two components whose interaction has promoted the strong starburst and disturbed morphology. It is interesting to note that both spectra have strong [N III]/Hα emission line flux ratios which may indicate that both components host active AGN.
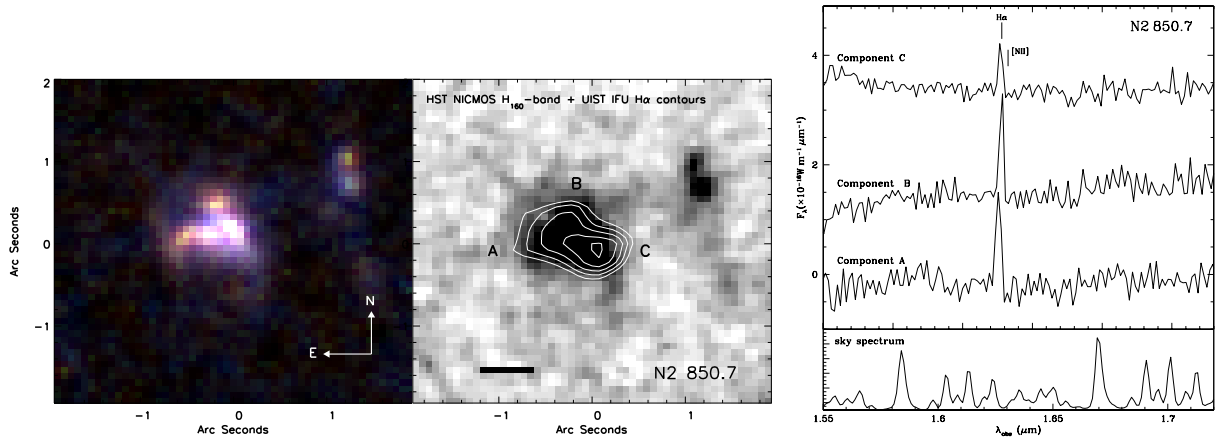

Figure 2. *Left:* A true colour image of N2 850.7 comprising *HST* ACS I_{814}-band and NICMOS H_{160}-band images illustrating the complex morphology of this system. *Middle:* NICMOS H_{160}-band image with Hα emission line intensity overlaid as contours. Each panel is 4 arcsec square (34 kpc at $z = 1.49$) and has East left and North top. The bar shown on the NICMOS image indicates the $0.6''$ resolution of the IFU observations. The system comprises at least three components, marked as A, B and C (and there is also tentative evidence for weak Hα emission from the source $\sim 1''$ to the West, suggesting it may be associated with the system). The continuum colours of C are bluer than the other components. The intensity of the Hα emission traces the H_{160}-band morphology and it is interesting to note that the star formation appears distributed across the SMG. *Right:* Spectra covering the redshifted Hα emission in the three components of N2 850.7 from the UIST IFU observations. The spectra have been offset in flux scale for clarity. The lower panel shows a sky spectrum. By centroiding the emission lines, we find velocity offsets between components A & B and A & C of 215 ± 80 km s^{-1} and 135 ± 90 km s^{-1} in projection respectively.
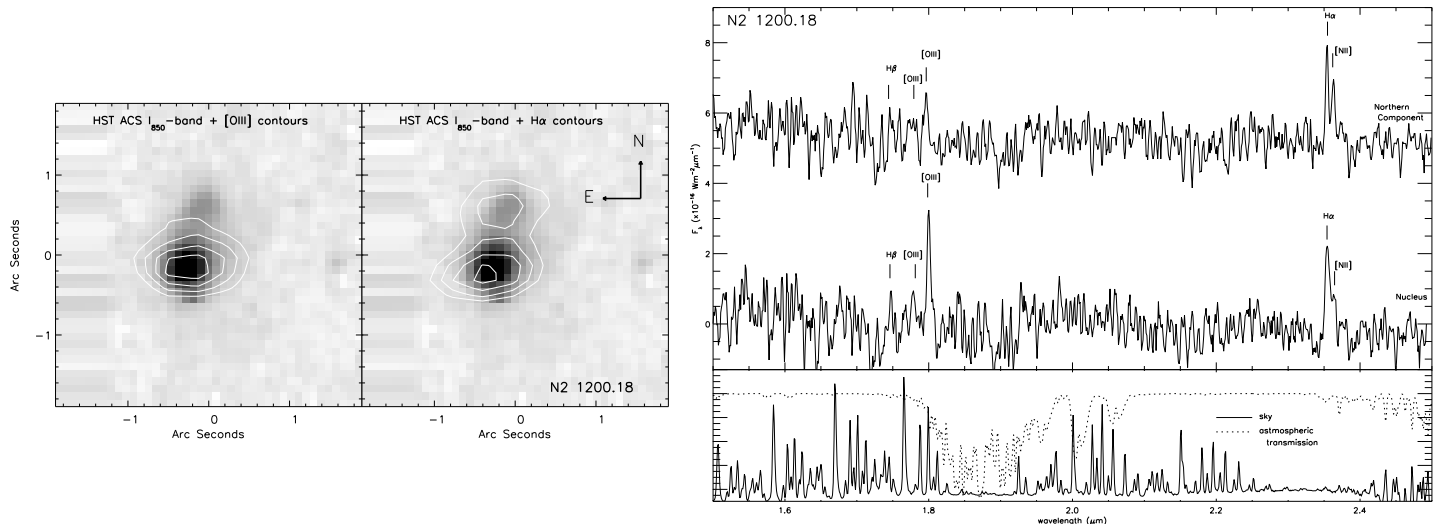

Figure 3. *Left:* *HST* I_{814}-band image of N2 1200.18 with the [O III]λ5007 and Hα emission line intensity maps from the UIST IFU observations overlaid as contours. Both panels are displayed on a log scale to emphasis the morphology. The *HST* image shows a a central bright, compact component and a lower-surface brightness extension to the North. The [O III]λ5007 and Hα emission also have different morphologies, with the strong, compact [O III]λ5007 probably arising from (unresolved) AGN activity in the bright central component, whilst the Hα morphology appears resolved and extends across the whole system. *Right:* Spectra from the central component and northern extension of N2 1200.18 around the [O III]λ5007 and Hα emission lines from the UIST IFU observations. The spectrum of the central source has an [O III]/Hα emission line flux ratio of 2.0 ± 0.5 which, combined with the unresolved [O III] emission suggests AGN activity. The northern component has a velocity offset of 250 ± 80 km s^{-1} from the nucleus. This northern component has star-burst (rather than AGN) characteristics, with a lower [O III]/Hα and [N II]/Hα emission line flux ratios. *Bottom:* The OH airglow emission from the sky (continuous line), as well as the Mauna Kea atmospheric transmission (dotted line) are also shown in the lower panel.
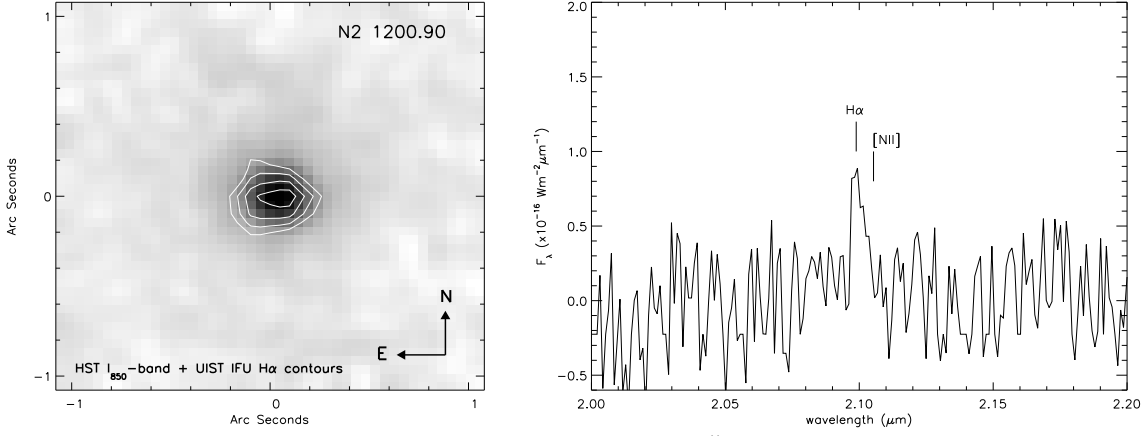
Figure 4. *Left: HST* I$_{814}$-band image of N2 1200.90. The galaxy has a compact morphology ($\lesssim 0.2''$ (1.6 kpc) FWHM) in this continuum imaging. *Right:* Spectrum of N2 1200.90 from the UIST IFU observations showing Hα at a redshift of $z = 2.198$. The rest-frame UV spectrum from Chapman et al. (2006) shows clear signs of AGN activity, yet the apparently low [N$_{II}$]/Hα emission line ratio from our near-infrared spectroscopy is more suggestive of star-formation. However, we note that the Hα emission line width of 500 ± 100 km s^{-1} may indicate (non-thermal) AGN activity.
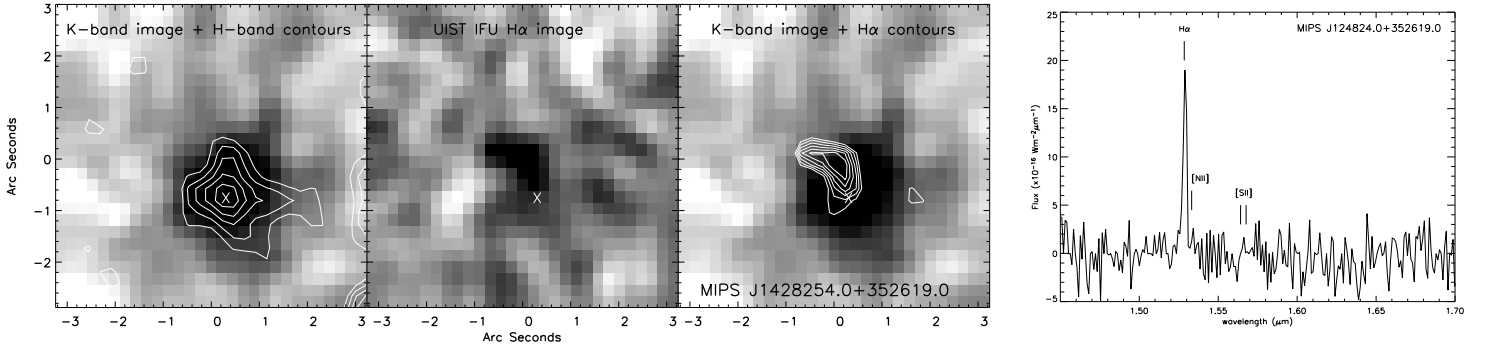
Figure 5. Images of MIPS J142824.0+352619 generated from the UIST IFU observations. *Left:* K-band continuum image (collapsed from the datacube between 2.0 and 2.4μm) with contours overlaid from the H-band (collapsed between 1.5 to 1.8μm). *Middle:* Continuum subtracted Hα image. *Right:* K-band image with contours from the continuum subtracted, Hα narrow-band image overlaid. The "X" in each panel marks the position of the center of the H-band light distribution. In the final panel we show the collapsed, one-dimensional spectrum around the redshifted Hα emission from MIPS J142824.0+352619. The Hα redshift of $z=1.328\pm0.003$ is in excellent agreement with the CO(5-4) emission, and the Hα line width and emission line flux are also comparable to those given in Borys et al. (2006).
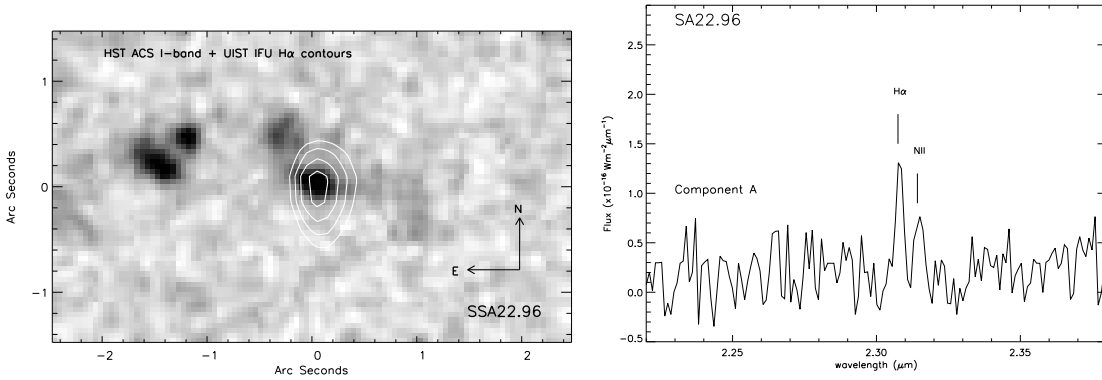
Figure 6. *Left: HST* I$_{814}$-band image of SA 22.96 with the Hα emission from the UIST IFU observations overlaid as contours. *Right:* Collapsed spectra around the Hα emission from the Western component (A) from the UIST IFU observations of SSA22.96. We identify A as the submm source at redshift $z=2.517$ through identification of strong Hα and [N$_{II}$] emission at the same redshift as derived from the rest-frame UV spectroscopy in Chapman et al. (2005). We note that there is tentative evidence for weak Hα emission from the structure $\sim 1.5''$ to the East, suggesting it may be associated with the system.

TABLE 1.
LOG OF IFU OBSERVATIONS

SMG	RA	Dec	z	$t_{exp}(ks)$
UIST/UKIRT				
SMM J163639.01+405635.9 (N2 850.7)	16:36:39.40	+40:56:38.0	1.4880	21.6
SMM J163655.80+405914.0 (N2 1200.18)	16:36:55.90	+40:59:12.0	2.5918	21.6
RG J163655.05+410432.0 (N2 1200.90)	16:36:55.05	+41:04:32.0	2.1981	14.4
MIPS J142824.0+352619.0	14:28:24.40	+35:26:21.8	1.328	21.6
SMM J221804.42+002154.4 (SSA 22.96)	22:18:04.43	+00:21:53.2	2.517	10.8
Gemini/GNIRS				
SMM J030227.73+000653.5 (CFRS 03.15)	03:02:27.6	+00:06:52.5	1.4076	7.2

Table 1. Note: The submm names/position give the 850μm centroid whilst the RA and DEC marked denote the 1.4GHz radio centroid.

[NII]/Hα and CIV/Lyα emission line ratios as well as a broad component underlying the Hα emission line (with FWHM of $2900 \pm 400\,\mathrm{km\,s^{-1}}$) from a partially obscured AGN (Chapman et al. 2005; Swinbank et al. 2004).

N2 1200.90: The 1.4-GHz map of the ELAIS-N2 field shows a slightly resolved source around this galaxy, with a peak flux density of $47 \pm 10\mu$Jy beam^{-1} and a total flux density of $63\pm21\mu$Jy (Biggs & Ivison 2006). A spectroscopic redshift $z = 2.195$ was measured through the identification of Lyα and CIV emission lines, the ratio of these suggests weak AGN activity is possible (Chapman et al. 2006).

MIPS J142824.0+352619: Far-infrared imaging with the *Spitzer* Space Telescope recently uncovered an apparently hyper-luminous galaxy at $z \sim 1.325$ (Borys et al. 2006). Multi-wavelength follow-up of this galaxy at submm wavelengths suggest a far-infrared luminosity of $3.2\pm0.7\times10^{13}$ L$_\odot$. Unlike most other $z > 1$ sources of comparable luminosity, MIPS J142824.0+352619 lacks any trace of AGN activity, and therefore the immense luminosity appears to arise due to a $\gtrsim 5000\,\mathrm{M_\odot yr^{-1}}$ star-burst. However, spectroscopic observations in the z-band have shown that this galaxy is aligned with a foreground $z=1.03$ elliptical galaxy, suggesting the possibility of gravitational amplification of the background source. This would provide a much more mundane explanation for the apparently immense luminosity of this galaxy.

SSA 22.96: Rest-frame UV spectroscopy of SSA 22.96 from Chapman et al. (2005) indicates a redshift of $z = 2.517$ from UV absorption features, with little indication of AGN activity. This radio pre-selected galaxy has $850\,\mu$m and 1.4 GHz flux densities of S$_{850}$=9.0$\pm$2.3mJy and S$_{1.4}$=43.8$\pm$10.1μJy which suggests a far-infrared luminosity of $L_{FIR} \sim 8\times10^{12}$ L$_\odot$.

Deconvolving the exact contributions from the star formation and AGN activity within these galaxies is difficult using just the UV slit spectroscopy from Chapman et al. (2005). Ideally we need to use the well-developed spectral indicators based on rest-frame optical emission lines (Veilleux & Osterbrock 1987) which fall in the near-infrared for these high-redshift galaxies (Swinbank et al. 2004). Going one step further, and coupling the spatial coverage from an IFU with coverage around the rest-frame optical emission lines allows us to locate and isolate the components hosting the AGN in these systems, determine dynamical masses, as well as searching for extended halos and/or companions.

2.2 UIST Near-Infrared Integral Field Spectroscopy

Spectro-imaging observations of five targets were made with the UIST near-infrared integral field spectrograph on UKIRT. The UIST IFU uses an image slicer to take a $3.3''\times6.0''$ field and divides it into 14 slices of width $0.24''$. The dispersed spectra from the slices are reformatted on the detector to provide 2-D spectro-imaging, in our case using the HK grism, at a spectral resolution of $\lambda/\Delta\lambda \sim 1000$ and covering a wavelength range of 1.4–$2.4\,\mu$m. N2 850.7 and N2 1200.18 we observed between 2004 August 20 and September 04, whilst the remaining targets were observed between 2005 June 25 and June 30[1]. All observations we taken $< 0.6''$ seeing and photometric conditions. Observations were carried out in the standard ABBA configuration in which we chopped by $12''$ to blank sky to achieve good sky subtraction. Individual exposures were 240 s and each observing block was 7.2 ks which was typically repeated two or three times, thus the total integration time for each object were 10–20 ks (Table 1).

To reduce the data we used the relevant ORAC-DR pipeline (Cavanagh et al. 2003) which sky-subtracts, extracts, wavelength calibrates, flat-fields, flux calibrates and forms the datacube. To accurately align and mosaic the individual datacubes together we created white light (wavelength collapsed) images around the redshifted Hα emission line from each observing block and used the peak intensity to centroid the object in the IFU datacube. We then spatially aligned and co-added the individual data-cubes to create the final mosaic.

2.3 GNIRS Integral Field Spectroscopy

We used the GNIRS IFU spectrograph to observe the $z = 1.4076$ submm galaxy CFRS 03.15[2]. The GNIRS IFU uses an image slicer to take a $3.2''\times4.8''$ field and divides it into 21 slices of width $0.15''$. By re-arranging the slices end-to-end at the detector, the IFU allows images to be dispersed into full length spectra whilst preserving the complete 2-D

spatial information content. This allows 3-D spectroscopy across a contiguous $3.2'' \times 4.8''$ field at $0.15''$ per pixel. We used the H-band filter with the 32 lines/mm grating which results in a spectral resolution of $\lambda/\Delta\lambda \sim 1700$ and records a wavelength coverage of between 1.37 and $1.87\mu m$. Observations were taken on 2005 October 20 in photometric conditions, but moderate ($\sim 1.0''$) seeing. We used the same observing strategy as with UKIRT: observations were carried out in the standard ABBA configuration in which we chopped away to sky by $12''$ to achieve good sky subtraction. Individual exposures were 600 s seconds and each of the ABBA observing blocks was repeated three times to give a total integration time of 7.2 ks. To flux calibrate the data, we observed the UKIRT standard star FS10. We used the Gemini IRAF package to extract, flat-field and wavelength calibrate the data and used IDL to build and combine the datacubes.

2.4   *HST* Optical and Near-Infrared Imaging

HST Advanced Camera for Surveys (ACS) observations of N2 850.7, N2 1200.18 were obtained from the *HST* public archive[3](Program ID #9761) whilst ACS images of SSA 22.96 was observed as part of Program #10145. The data consist of dithered exposures with the F814W filter, taken in LOWSKY conditions using the default four-point ACS-WFC-DITHER-BOX configuration. This pattern ensures optimal half-pixel sampling along both coordinates. The typical integration time were 4.8 ks. We reduced the data using the latest version of the MULTIDRIZZLE software (Koekemoer et al. 2002) using the default parameters with PIXFRAC=1 and SCALE=1. The resulting images have $0.05''$ pixels and are free from artifacts. Further details of these observations are given in Borys et al. (2006b) (see also Almaini et al. 2005).

   HST WFPC2 observations of CFRS 03.15 were also obtained from the *HST* public archive. The data were taken in the F814W and F450W filters for total of 1.4 ks each (Program ID #05996 and #06556). These observations were reduced using the standard STSDAS package in IRAF.

   HST NICMOS observations of N2 850.7 and CFRS 03.15 were obtained in Cycle 12, and the targets were observed using the NIC2 camera in the F160W filter for a total of 2.3 ks (Program ID #9856). We employed the standard four point spiral dither pattern, LOWSKY conditions and used the MULTIACCUM read-mode.

Each exposure was corrected for a pedestal offset, and then mosaiced using the CALNICB task in IRAF. Unfortunately the observation was affected by the South Atlantic Anomaly (SAA), and extra processing steps were required[4]. The final images appear very flat and have very low cosmic ray contamination. The reduction and analysis of these data is described in more detail in Borys et al. (2006b).

3   ANALYSIS & RESULTS

3.1   Velocity Determinations

To accurately determine the redshift (or velocity offsets between components) in the spectra, we identify and fit both the continuum level and emission lines (e.g. $H\alpha\lambda 6562.8$, and $[NII]\lambda\lambda 6548.1, 6583.0$ where appropriate) simultaneously with a flat continuum plus Gaussian profiles using a χ^2 fit and taking into account the increased noise in regions of strong sky emission. The error bars on the emission-line wavelength in each spectrum are derived by allowing the wavelength of the best-fit Gaussian profile to vary and allowing the signal to drop by $\Delta\chi^2 = 1$. The quoted error-bars are therefore conservative and reflect the signal-to-noise of the data. The velocity error is propagated through to the mass determinations in §4. However, since the signal-to-noise in some of our observations is modest we also attempt to further quantify the error-bars on the velocity offsets by creating artificial emission lines at the resolution of the UIST spectrograph. We produce spectra with emission lines with an intrinsic width of $150\,km\,s^{-1}$ and add Gaussian random noise. We then refit the Gaussian profiles to the data, measuring the velocity offset betwen the input and output spectrum. Using 10^4 simulations at each signal-to-noise, the rms velocity error between the measured fit and the input velocity as a function of signal-to-noise (S/N) is: $140\,km\,s^{-1}$ at S/N=3, $100\,km\,s^{-1}$ at S/N=5, $65\,km\,s^{-1}$ at S/N=7 and $50\,km\,s^{-1}$ at S/N=9. As expected, these estimates are comparable to the quoted velocity errors derived using our χ^2 estimate.

   Before we discuss what can be learnt from our observations as a whole, we briefly review the results from each of the six galaxies.

3.2   CFRS 03.15

In Fig. 1 we show a true colour BIH-band *HST* image of CFRS 03.15. The galaxy shows a compact source surrounded by a diffuse halo of material in a ring-like structure. The colours of the nucleus ($B_{450} - I_{814}$=1.8 $I_{814} - H_{160}$=2.5) are consistent with a star forming galaxy at $z = 1.407$, although the "ring" of material surrounding the nucleus is much redder in $(B - I) \gtrsim 3.5$, but bluer in $(I - H) = 1.8 \pm 0.2$, suggesting that $[OII]\lambda 3727$ emission (λ_{obs}=8973Å) may be contributing significantly to the I-band flux. There is also a compact knot (or companion) approximately $1.5''$ (12.5 kpc) to the South-West with similar colours to the nucleus.

   From our datacube we construct a wavelength-collapsed $H\alpha$ image (collapsed between -300 and $+300\,km\,s^{-1}$ from

the systemic redshift of Chapman et al. 2005) and overlay this on the NICMOS H-band image (Fig. 1). The H-band and Hα morphologies are well matched, and we confirm that the bright knot located $\sim 1.3''$ (~ 11 kpc) to the South-West is associated with the galaxy (the extended Hα morphology and Hα velocity shear was also tentatively detected in the Keck/NIRSPEC spectrum in Swinbank et al. (2004) in which the longslit was placed across both components). Since the observations were taken in $\sim 1''$ seeing, we cannot discuss the small scale properties of each component in detail (or confirm the nature of the low surface brightness halo of diffuse material surrounding component A), however, these will be discussed in Blain et al. (in prep) who use Laser Guided Adaptive Optics assisted H-band Keck/OSIRIS IFU observations of this system.

By extracting spectra from around the two brightest components we identify a velocity offset between the nucleus and the knot of $90\pm20\,\mathrm{km\,s^{-1}}$. We note that the [N II]/Hα emission line flux ratios of components A and B are both high (0.95 ± 0.05 and 1.05 ± 0.05 respectively), suggesting that both components may host active AGN. In order to further search for signatures of non-thermal activity, we attempt to fit each of the spectra with an underlying broad-line component, but the improvement in χ^2 over just fitting [N II]+Hα+[N II] is not significant.

3.3 N2 850.7

We detect Hα emission at 1.630μm (in agreement with the UV and Hα redshift from Chapman et al. 2005 and Swinbank et al. 2004) and construct an Hα image of N2 850.7 by collapsing the datacube between 1.620 and 1.640μm. In Fig. 2 we show the *HST* NICMOS image of N2 850.7 and overlay on this the Hα image from the IFU observations. The Hα morphology of the central components is spatially extended and therefore to search for velocity sub-structure, we extract spectra from the regions in the IFU datacube around the brightest components seen in the *HST* imaging. From each individual component, the signal-to-noise of the Hα emission is only modest; nevertheless, it is sufficient to centroid the Hα emission line in all cases and so search for velocity offsets between components. We identify a velocity offset between components A and B of $215 \pm 80\,\mathrm{km\,s^{-1}}$ and an offset between A and C of $135 \pm 90\,\mathrm{km\,s^{-1}}$. The *HST* imaging and velocity offsets suggest that at least two galaxies are undergoing an interaction, although whether component C belongs to the same structure as B (or A) will have to wait for higher resolution (adaptive optics) IFU observations. We note that the continuum colours of A, B and C are very similar (Smail et al. 2004).

Using the Hα luminosity as a star-formation rate indicator, we derive star-formation rates of 90 ± 20, 70 ± 20 and 60 ± 20 M$_\odot$yr^{-1} from components A, B and C respectively (Kennicutt 1998). In comparison, the star-formation rate for the whole system from the far-infrared luminosity is 1100 ± 300 M$_\odot$yr^{-1}, implying ~ 2 magnitudes of extinction (q.v. Smail et al. 2004). We reiterate that neither the emission line flux ratios from the IFU observations nor the restframe UV spectroscopy from Chapman et al. (2005) show any signs of AGN signatures.

3.4 N2 1200.18

The *HST* I_{814}-band ACS image of N2 1200.18 ($z = 2.5918$) appears complex with a bright knot and a low-surface-brightness extension or companion approximately $0.7''$ (6 kpc) to the North. Since the IFU observations of this galaxy cover Hβ, [O III]$\lambda5007$ and Hα, we construct wavelength-collapsed images around the [O III]$\lambda5007$ and Hα emission lines and overlay these on the NICMOS H_{160}-band image in Fig. 3. The strongest [O III]$\lambda5007$ emission appears to come from an unresolved point source in the central, bright I_{814}-band continuum component. In contrast, the Hα is much more extended and has features which match the extended Northern component seen in the I_{814}-band. This suggests that the compact continuum source may host an AGN and indeed, both the strong, spatially unresolved [O III]$\lambda5007$ and high [O III]$\lambda5007$/Hα(=2.0 ± 0.5) and [N II]/Hα(=0.7 ± 0.1) emission line ratios suggest AGN activity. We note that the Hα/Hβ emission line flux ratio of the central and northern components are 8 ± 3 and >5 respectively.

We can use the emission line flux ratios of [O III]/Hβ and [N II]/Hα of N2 1200.18 to classify the two components seen in the UIST IFU data. The northern component has an [N II]/Hα emission line flux ratio of 0.6 ± 0.1, and an [O III]$\lambda5007$/Hβ ratio of 0.5 ± 0.2, together these place this component it in the LINER region of the diagnostic diagrams of Baldwin et al. (1981). The high [O III]$\lambda5007$/Hα and [N II]/Hα emission line flux ratios from the central unresolved component, indicate a Seyfert-2 type AGN.

Using the velocity derived from the Hα emission, we find that the unresolved central component is redshifted from the northern extended component with a velocity offset of $250 \pm 100\,\mathrm{km\,s^{-1}}$ across $0.8''$ (~ 7 kpc) in projection.

Using deep *Chandra* observations of the ELAIS N2 field it is also possible to compare the X-ray and spectral properties of N2 1200.18. This galaxy is detected in the hard (2–8 keV) X-ray image with a flux of $14.7 \pm 2.1 \times 10^{-15}\,\mathrm{erg\,s^{-1}\,cm^{-2}}$ (Manners et al. 2003). We convert the observed 2–8 keV flux to a rest frame 2–10 keV luminosity using the equations from Alexander et al. (2003b) assuming a spectral index Γ=2. We derive L_X=$9.1\pm1.3\times10^{44}\mathrm{erg\,s^{-1}}$. Under the assumption that the [O III]$\lambda5007$ emission line and the hard X-ray fluxes are isotropic, they can be used to investigate the intrinsic power of Seyfert galaxies (Mulchaey et al. 1994; Alonso-Herrero et al. 1997). N2 1200.18 sits comfortably in the scatter of the L$_{[OIII]}$–L$_X$ plot for local Seyferts from Mulchaey et al. (1994), although it lies at the high luminosity end, furthering the suggestion that N2 1200.18 hosts a high luminosity Seyfert 2 AGN, and also suggesting that increased AGN activity results in increased photo-ionization of the surrounding material. This source, along with low-resolution spectroscopy of the [O III]5007 emission from a larger sample of submm galaxies, is discussed in detail by Takata et al. (2006).

3.5 N2 1200.90

The *HST* I_{814} image of this galaxy shows a compact morphology ($\lesssim 0.2''$ (1.6 kpc) FWHM), which is matched by the Hα morphology from the UIST IFU observations. The Hα emission from this galaxy is spatially unresolved and we de-

tect no significant velocity structure across the galaxy. The line width of the Hα emission is $420\pm100\,\mathrm{km\,s}^{-1}$ and the integrated line flux of $0.5\times10^{-18}\,\mathrm{Wm}^{-2}$ then suggests a SFR of $150\pm50\,\mathrm{M}_\odot\mathrm{yr}^{-1}$ (Kennicutt 1998).

3.6   MIPS J142824.0+352619

The discovery that there is a fortuitous alignment of a massive foreground elliptical galaxy at $z{=}1.03$, superimposed onto the $z{=}1.325$ far-infrared-luminous galaxy (Borys et al. 2006) suggests the possibility that MIPS J142824.0+352619 may be gravitationally lensed. To this end, we targeted the Hα emission with the UIST IFU in order to search for morphological signatures of strong lensing which might explain the apparent immense luminosity of MIPS J142824.0+352619.

In Fig. 5 we show the continuum subtracted Hα emission line map of MIPS J142824.0+352619 overlaid on the K-band continuum image generated from the IFU. The Hα emission is spatially extended, across $\sim1''$ in projection, however, the H and K-band light is much more widely distributed, showing likely contamination by light from the foreground lens. The Hα emission appears elongated, but with an alignment which is not naturally ascribed to gravitational lensing (we would expect the brightest images to straddle the long-axis of the foreground lens potential). To search for velocity structure, we extract a series of independent spectra from the datacube along the arc, and place a limit of $\lesssim125\,\mathrm{km\,s}^{-1}$ on any possible velocity shear. We show the collapsed, one-dimensional spectrum around the Hα emission in Fig. 5. The lack of velocity structure may be a further indication that the Hα morphology arises from two merging images of the same background source, with the third (much lower surface brightness) image undetectable to the South West. Whilst such a lens model is somewhat contrived, it would potentially yield an amplification $\gg10$ for the background source.

3.7   SSA 22.96

The *HST* ACS I-band imaging of SSA 22.96 shows several components around the submm galaxy (labelled A). Component A is the radio counterpart in the 1.4-GHz map from Chapman et al. (2004). To align the IFU datacube with the optical imaging we construct a Hα image of SSA 22.96 by collapsing the datacube between 2.29 and $2.33\mu m$ and overlay this on the *HST* I_{814}-band image in Fig 6. We extract a spectrum from the datacube around the position of the submm galaxy and also show this in Fig. 6. The Hα redshift of component A is in excellent agreement with the UV redshift from Chapman et al. (2005).

The rest-frame UV spectroscopy from Chapman et al. (2005) is measured from absorption lines, yet the high [N$\textsc{ii}$]/Hα emission line flux ratio (0.6 ± 0.2) we see may be more consistent with either high metallicity or AGN activity (Veilleux & Osterbrock 1987). We note that this galaxy is not detected in the archival 0.4–10 KeV XMM X-ray image of this field to a flux limit of $6\times10^{-15}\mathrm{erg\,s}^{-1}\,\mathrm{cm}^{-2}$ (which corresponds to $\mathrm{L}_X<3\times10^{44}\mathrm{erg\,s}^{-1}$).

4   DISCUSSION

In this paper, we have spatially mapped the rest-frame optical line emission in a sample of six high redshift, luminous submm galaxies. We also include in our discussion two similar galaxies which also have published IFU observations (N2 850.4 and SMMJ 14011+0252; Swinbank et al. 2004; Tecza et al. 2004). The most striking feature in the combined sample of eight submm galaxies is the prevelance of galactic-scale multiple components: five of the eight appear to comprise two or more galactic-scale extensions/components on 1–2$''$ (8–16 kpc) scales. Our IFU observations also show that velocity structures can be identified within individual components (e.g. on $\lesssim0.5''$, 4 kpc scales).

Such velocity structures are not only observed through the nebular emission: recently Greve et al. (2005) and Tacconi et al. (2006) have published mm-wavelength observations of twelve submm galaxies. Several of these systems show double-peaked CO emission line spectra, with velocity offsets of up to $800\,\mathrm{km\,s}^{-1}$ and line widths of up to $1000\,\mathrm{km\,s}^{-1}$ (FWHM). The individual CO peaks often have similar intensities ($I_{CO_1}/I_{CO_2}{=}0.7\pm0.1$ with a range of $I_{CO_1}/I_{CO_2}{=}0.3$–0.9) suggesting that many of the submm galaxies could contain massive gas disks (Genzel et al. 2003). This interpretation is supported by examples of ULIRGS with gas rich disks in the local Universe (e.g. NGC 6240; Tacconi et al. 1999). However, the obvious interacting/merger nature of many of these distant submm galaxies from our *HST* and IFU observations strongly suggests that the velocity offsets we measure arise from merging systems. The IFU observations also show that the components have large differences in their energetics and AGN contributions over 2–20 kpc scales. interpretation is supported by recent observations of

4.1   Mass Estimates

Constraining the stellar, gas and dynamical masses of submm galaxies is crucial if we are to understand their evolution. Recent dynamical masses for SMGs from CO spectroscopy with millimetre interferometers indicate a dynamical mass of $\log(\mathrm{M}_{dyn}) = 11.1 \pm 0.3$ and gas masses of $\log(\mathrm{M}_{gas}) = 10.5 \pm 0.2$ within the central $\sim10\,\mathrm{kpc}$ (Greve et al. 2005; Tacconi et al. 2006). In addition, estimates of the stellar masses for submm galaxies have been given by Borys et al. (2005). These are derived by fitting simple stellar population models to the spectral energy distributions of submm galaxies across the restframe ultraviolet, optical and near-infrared wavebands. The inclusion of restframe near-infrared data into these fits improves their insensitivity to dust extinction and thus provides much more reliable measures of the luminosity of the stellar populations in these systems. In this way, Borys et al. (2005) derived a median stellar mass of $\log(\mathrm{M}_*) = 11.4 \pm 0.4$ for a small sample of spectroscopically identified submm galaxies in the GOODS-N region.

We are also able to place limits on their dynamical masses in this population using the projected velocity offsets and spatial separations in our IFU observations. In Fig. 7 we construct a velocity offset versus spatial offset diagram for all submm galaxies which show multi-components in their spatially resolved spectra, either from IFU spectroscopy

(this work; Swinbank et al. 2005; Tecza et al. 2004); resolved CO spectroscopy (Greve et al. 2005; Tacconi et al. 2006); or longslit observations (Swinbank et al. 2004). We note that no two data-points in Fig. 7 represent the same sub-mm galaxy: the only multi-component SMG which has both CO and IFU observations (N2 850.4) is represented by an IFU data-point in the figure (the measured kinematics in N2 850.4 from IFU and CO observations give consistent results and are discussed in Swinbank et al. (2005); see also Tacconi et al. (2006)).

To investigate the masses of these systems we assume that the velocity offsets between the different components eventually transform into motions in a single, relaxed potential well, i.e. they reflect virial motions. We therefore overlay the expected projected velocity dispersion as a function of radius for an elliptical galaxy with an NFW profile (Navarro et al. 1997; Łokas & Mamon 2001). We assume a concentration of $c = 7$ and a virial radius of 200 kpc – typical of a massive elliptical galaxy (Mamon & Łokas 2005; Romanowsky et al. 2003). Interpreting the velocity offsets in this way, we derive a median dynamical mass of $5\pm3\times10^{11}$ $M_\odot$ within the virial radius for these galaxies.

Before we compare the dynamical mass estimates with the stellar and gas masses, we note first that there are clearly uncertainties in applying the virial theorem and attempting to measure the mass of a (non-stationary) merging systems. The following caveats must be considered:

1) Whilst these are merging systems and out of equilibrium, the virial theorem may still be applied if an extra term is included to reflect the moment of inertia of the system (d^2I/dt^2): such that $2T+W=d^2I/dt^2$. Since the moment of inertia is strongly weighted towards large radii ($I \propto \int r^2 dm$), relatively minor parts of the galaxy (such as tidal tails) can have a large impact on I and hence the virial mass estimate. However, in many of these systems, the velocity dispersions (and star-formation activity) of the individual components (and the fact that two SMGs appear to comprise double AGN) suggest that we are not measuring velocities for "minor" components, but rather these are likely to be the dominant components of the merger.

2) The virial theorem is strictly only valid if the components we observe follow the distribution of mass in the galaxy. Since the components we measure are the likely nuclei of the progenitor galaxies they will be more concentrated (due to dynamical friction) than the overall mass distribution and may produce an underestimate of the dynamical mass.

3) The virial theorem should only be applied if the merging components have similar mass ratios. The velocity dispersions (and star formation activity) of the individual components we measure are often comparable arguing that the mass ratios of the merging components are similar. It is also useful to note that recent observations of local ($z \lesssim 0.1$) ULIRGs which have shown that galaxies with $L \gtrsim 10^{12}$ $L_\odot$ typically comprise systems two (or more) interacting components with mass ratios 1:1 to 1:3 (Dasyra et al. 2006).

To gauge the validity of the mass estimate from the virial theorem, we can make a further estimate of the dynamical masses: if we take the velocity offsets and assume these are point masses (i.e. assume $M = \Delta v^2/\Delta rG$), we derive masses of $2.5\pm1.5\times10^{11}$ $M_\odot$. We view this estimate as more uncertain than that using the virial estimator since

this estimate requires placing all of the mass of the progenitors into point masses on circular orbits. The estimate based on the point-mass model is within the range we quote, and so we consider $5\pm3\times10^{11}$ $M_\odot$ a reasonable estimate of the mass and its uncertainty in the typical submm galaxy in our sample. However, we note that these estimates would benefit considerably from (high angular resolution) adaptive optics IFU observations coupled with a theoretical study of the distribution of detectable emission line gas within dusty, merging systems at high redshifts.

4.1.1 Comparison with Stellar Mass Estimates

Borys et al. (2005) estimated restframe 2.2-μm luminosities for a sample of spectroscopically-confirmed submillimetre galaxies in the GOODS-N region from broad-band photometry covering $UBVRIzJK$+IRAC 3.6/4.5/5.8/8μm – which spans the restframe UV, optical and near-infrared at the redshifts of their sample, $z = 0.56$–2.91. They find $M_K = -26.8 \pm 0.4$ from their sample of 10 galaxies at $z > 1.5$. They then adopted a typical light-to-mass ratio for the stellar population of L_K/M=3.2, based on an estimated mean age of ~ 250 Myrs from fitting simple stellar population models to the broad-band SEDs, and so derive typical stellar masses of $\log(M_*) = 11.4 \pm 0.4$ (Borys et al. 2005). This is a significant stellar mass for a galaxy at $z \sim 2$ and so Borys et al. (2005) discuss in detail the potential uncertainties in their estimates, in particular whether it is possible to reduce the stellar masses. The most obvious way to achieve this would be to adopt a higher L_K/M ratio, equivalent to assuming a younger age for the stellar population. However, to achieve an order-of-magnitude reduction, i.e. a light-to-mass ratio of $L_K/M \sim 30$, would require a typical age of ~ 10 Myrs (Leitherer et al. 1999). Given the observed space density of submillimetre galaxies, such very young ages and hence high-duty cycles imply very large volume densities for the progenitor population ($\sim 10^{-3}$ Mpc^{-3}) which is at least an order of magnitude greater than the estimates of the masses and clustering of this population (Blain et al. 2004; Chapman et al. 2005).

It is also possible that AGN contribute to the measured 2.2-μm luminosities, leading to an over-estimation of the stellar masses. As Borys et al. (2005) point out, the shape of the spectral energy distributions for typical submillimetre galaxies is well-described by a stellar model and indeed they remove from their analysis the small number of galaxies for which an AGN is potentially dominant in the restframe near-infrared. Nevertheless, we can take an extreme view point and ask if AGN produce all of the luminosity in the reddest bands in these sources, how much would that influence the estimated stellar luminosity? We use the average near-infrared spectral index for QSOs from Simpson & Rawlings (2000), $\alpha = 0.98$, assume that all of the observed 8.0-μm luminosity is arising from the AGN and estimate its contribution to the luminosity at a restframe wavelength of $\sim 1.6\mu$m (where the stellar contribution should peak). Using this set of extreme assumptions, we find a median reduction in the stellar luminosity of only 4$\times$, suggesting that a more realistic estimate taking into account the stellar contribution at 8.0μm, is likely to yield a change of $\lesssim 2\times$, within the error range quoted by Borys et al. (2005). It is also worth noting at this point that Alexander et al. (2005) have shown that
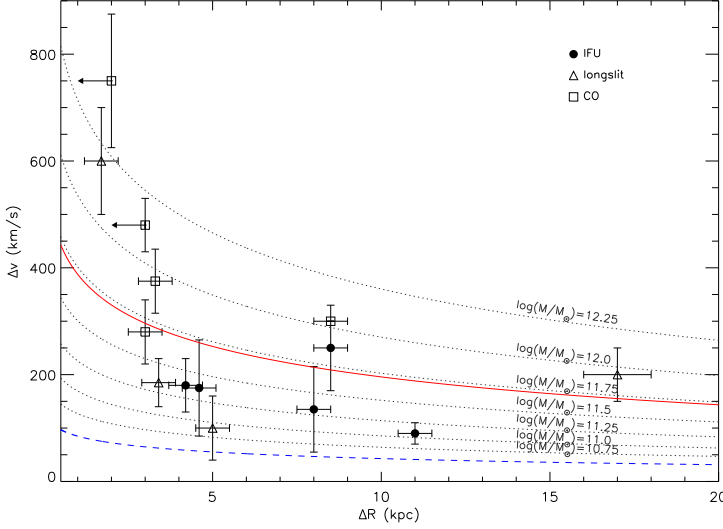
Figure 7. Velocity offset versus spatial offset for the multiple components within submm galaxies from IFU, longslit or CO observations. The dotted lines show the expected profiles as a function of halo mass for a galaxy with an NFW profile and a concentration parameter typical of elliptical galaxies. Treating the observations as an ensemble, we derive a dynamical mass for the SMGs of $M=5\pm3\times10^{11}$ $M_\odot$ (shown by the solid line). For comparison, the dashed line shows the profile for the minimum stellar mass derived from Borys et al. (2005).

while AGN are ubiquitous in SMGs, their typical contribution to the bolometric emission is $\lesssim 10\%$ suggesting that any contamination to the 2.2μm flux from AGN activity is minimal and unlikely to bias our result.

Finally, we note that recent stellar population synthesis modelling by Maraston et al. (2006) has shown that thermally pulsating asymptotic giant branch (TP-AGB) stars in post starburst galaxies can contribute significantly to the rest-frame K-band luminosity on $\gtrsim 200$–1000Myr timescales. Indeed, the predicted stellar light-to-mass ratios at 250 Myr is $L_K/M\sim 6$–8 (Maraston 1998; Maraston et al. 2006) and therefore may act to reduce our estimated stellar mass by a factor of up to $3\times$ if the luminosity weighted stellar populations in the SMGs are dominated by stars with ages of $\gtrsim 200$–1000Myr. However, in the case of an on-going starburst (as is relevant for SMGs) the importance of TP-AGB phase is likely to be lessened and we estimate a maximum of $L_K/M\sim 5$ at 450 Myr and more typically $L_K/M\lesssim 4$ for the likely ages of SMGs, suggesting that this phase is unlikely to bias our results significantly.

Hence, unless there is a conspiracy between a number of factors, it appears unlikely that the estimated stellar masses for the submillimetre population are over-estimated by more than a factor of 2–3$\times$. We conclude therefore that the typical stellar and dynamical masses for submillimetre galaxies are likely to be similar in magnitude. We estimate a mass ratio of $M_{dyn}/M_* \sim 2$, with a considerable uncertainty. This suggests that, as with local luminous ellipticals, the central regions of these galaxies are baryon-dominated.

4.2 Space Densities and Comparison with Local Populations

In order to test the connection between SMGs and local galaxy populations we can evolve their stellar populations to the present day and determine whether their descendents would be consistent with scaling relations for local galaxies, such as the Faber-Jackson relation (Faber & Jackson 1976). This will test claims that SMGs evolve into massive ellipticals at the present day (e.g. Lilly et al. 1999). The velocity offsets we measure in §4.1 implies an average velocity dispersion of approximately $\sigma = 240 \pm 80\,\mathrm{km\,s^{-1}}$. The Faber-Jackson (FJ) relation for local early-type galaxies indicates that this dispersion corresponds to an r-band magnitude of $M_r = -22.7 \pm 0.5$ (Bernardi et al. 2005) or $M_K = -25.3 \pm 0.5$ (assuming $(r - K) = 2.6$, typical for an elliptical galaxy at the present day). Is the expected fading of the stellar populations within the SMGs, with $M_K = -26.8 \pm 0.4$ at $z \sim 2$, sufficient to reconcile them with the $z = 0$ FJ relation?

The key to estimating the degree of fading of the SMGs is to determine the likely ages of the stellar populations. Since the starburst lifetimes in SMGs depends on the mass of the molecular gas reservoir and the star-formation rate, Greve et al. (2005) used CO(3-2) transitions for 18 SMGs (and assuming a CO–H$_2$ conversion factor) to infer gas masses, obtaining $M(H_2) \sim 3 \times 10^{10}$ M$_\odot$. Recently, Hainline et al. (2006) have reported CO(1-0) observations of an SMG using the Green Bank Telescope and derive a H$_2$ gas mass four times larger than that from the CO(4-3) transition of the same source (implying that $J_{upper} >3$ transitions of CO significantly underestimate the mass of cold, diffuse molecular gas in SMGs). This suggests that the typical gas masses of SMGs are likely to be $M(H_2) \sim 1 \times 10^{11}$ M$_\odot$. Star formation rates can be derived from the bolometric emission of the source, assuming this is powered by star formation. Greve et al. (2005) used $850\,\mu$m and $1.4\,$GHz fluxes and assumed the far-infrared-radio correlation to determine bolometric luminosities for their sample. They then assumed a conservative contribution of 50% to the bolometric luminosity from a AGN, and so estimated a median star-formation rates of 700 M$_\odot$yr^{-1} for the galaxies in their sample (integrating the Salpeter IMF between 1 and 120M$_\odot$yr^{-1}). Two recent results influence this conclusion, but essentially leave it unchanged. Firstly, Alexander et al. (2005) have shown that while AGN are ubiquitous in SMGs, their typical contribution to the bolometric emission is $\lesssim 10\%$, which would increase the star-formation rate estimated by Greve et al. (2005) by $\sim 2\times$. However, Kovacs et al. (2006) have used $350\,\mu$m photometry to improve the estimates of the bolometric luminosities from the far-infrared SEDs of SMGs and show that the star-formation rates may be overestimated by a factor $\lesssim 2\times$, cancelling this increase. Hence, our current best-estimate of the gas consumption timescales in SMGs is: $\tau_{\mathrm{SMG}} \sim M(H_2)/SFR \sim 1 \times 10^{11}$ M$_\odot$ /700 M$_\odot$yr$^{-1}\sim$ 150 Myr, although this estimate clearly has significant uncertainties. The reader should note that a burst with this duration and star-formation rate can account for all of the observed stellar mass in a typical SMG, suggesting that the activity we are witnessing is likely to be the origin of the majority of the stellar mass in these galaxies (Smail et al. 2004).

We can next compare these burst lifetimes with those required in order for the SMGs to lie on the FJ relation at the present day using stellar synthesis modelling. For SMGs with $z > 1.5$, the average rest-frame K-band magnitude from Borys et al. (2005) is $M_K = -26.8 \pm 0.4$. We start by calculating the fading of a simple instantaneous burst to the present day. We use STARBURST99 (Leitherer et al. 1999) with a Salpeter IMF (Salpeter 1955) and an instantaneous star-burst which predicts that between 100 Myr and 10 Gyr there should be approximately $\Delta M_K = 3.4$ mags of fading suggesting the present day descendants should have $M_K \sim -23.4 \pm 0.4$. This is approximately 2 magnitudes fainter than the FJ relation, given the expected velocity dispersion as found in §4.1. Similarly, an instantaneous burst using the models of Maraston et al. (2006) suggests that the fading between 100 Myr and 10 Gyr is approximately $\Delta M_K = 2.1$–2.4 (depending upon the metallicity) – which is still $\gtrsim 0.6$ magnitudes fainter than the FJ prediction, given our expected velocity dispersion.

However, these instantaneous burst models are unphysical for SMGs which are still forming stars at the current epoch. So, we derive the fading from a more realistic model: a constant burst of star-formation of duration 100, 200 and 300 Myrs using PEGASE (Le Borgne et al. 2004). For a 100 Myr burst (observed at 50 Myr, since we expect on average to see SMGs half way through their active phase) the fading between the epoch of observation and the present day is $\Delta M_K = 3.2$, ~ 1.5 magnitudes too faint compared to the FJ relation for the velocity dispersion. Taking longer burst durations of 200 and 300 Myrs (observed at 100 and 150 Myr respectively) the fading is $\Delta M_K = 2.7$ and 2.3 magnitudes respectively – approximately 1.2 and 0.8 magnitudes off the FJ relation. Thus for our preferred burst lifetime, 300 Myrs, observed half way through the burst, the predicted present-day magnitude is $M_K \sim -24.5 \pm 0.4$ compared to the $z = 0$ value of $M_K = -25.3 \pm 0.5$ from the FJ relation.

These predictions are of course sensitive to the choice of IMF, changing from a Salpeter to a Kroupa IMF and for a 300-Myr burst the predicted fading reduces to $\Delta M_K = 1.7$, indicating a present-day luminosity of $M_K \sim -25.1 \pm 0.4$ and placing the SMGs within ~ 0.2 magnitudes of the $z = 0$ FJ relation. We note that such a change would be at odds with the "top-heavy" IMF needed in semi-analytic models of galaxy formation to reproduce the basic properties of SMGs (e.g. Baugh et al. 2005; see also Blain et al. 1999b,a).

Hence, whilst there are a number of uncertainties in estimating both the starburst lifetimes and the fading of SMGs to the present day, longer burst durations (~ 300 Myrs) are favoured in order for SMGs to evolve towards the scaling relations for elliptical galaxies at the present day. Burst timescales of this length are also consistent with the expected time to consume the gas reservoirs in these galaxies and with the build up of the present stellar mass in the systems.

We can also investigate how the SMG burst lifetimes influence the space densities of their expected descendants at the present day. The full SMG redshift distribution from Chapman et al. (2005) is well fit by a Gaussian with a mean redshift of $< z >= 2.2$ and a with, $\sigma_z \sim 1.3$ (accounting for incompleteness in the spectroscopic desert). Thus the SMGs populate an epoch of about $\tau_{obs} = 1.5$ Gyr in duration. Since $\phi = \rho_{SMG} \tau_{obs} / \tau_{burst}$ (where ϕ is the comoving space density

of the descendant population, $\tau_{\rm burst}$ is the burst lifetime, and $\rho_{\rm SMG}$ is the observed space density) an estimate of $\tau_{\rm burst}$ allows us to infer ϕ. We first estimate the observed space density ($\rho_{\rm SMG}$) by taking the observed surface density of >5 mJy SMGs from Chapman et al. (2005) (~ 1000 per square degree) which suggests that between $z = 0.9$–3.5 the volume density should be $\sim 2.5 \times 10^{-5} {\rm Mpc}^{-3}$ (this calculation assumes that 67% of the SMGs lie within the 1σ limits and includes the incompleteness correction in both the redshifts and radio-detection limits). Using our estimated lifetime of $\tau_{\rm burst} \sim 300$ Myr, the corrected space density (assuming a galaxy only goes through one SMG phase in its lifetime) is therefore $2.5 \times 10^{-5} \times 1.5$ Gyr/300 Myr $\sim 1.3 \times 10^{-4} {\rm Mpc}^{-3}$ for a population with predicted present day K-band absolute magnitude of $M_K \sim -25.1$. Integrating down the $z = 0$ luminosity function of early-type galaxies from Croton et al. (2005) (see also Wake et al. 2006), to a median magnitude of $M_K \sim -25.1$ we determine a space density of $9 \times 10^{-5} {\rm Mpc}^{-3}$ (we note that using the LRG luminosity function from Wake et al. 2006 we obtain 1.1. $\times 10^{-4} {\rm Mpc}^{-3}$). Thus if SMGs have burst durations of approximately 300 Myr, as indicated by their gas consumption timescales, then their predicted fading would place them on (or near-to) the present day FJ relation and the observed space density of this population at $z \sim 2$ (corrected for the duty-cycle of the bursts) would account for the formation of the whole population of early type galaxies with $M_K < -25.1$, ($\gtrsim 3L_K^*$) seen at $z \sim 0$.

Further evidence for the evolution of SMGs into massive ellipticals has also be presented in Tacconi et al. (2006) who used high resolution millimeter imaging to derive matter volume and surface densities of $\sim 100 {\rm cm}^{-3}$ and $5000 {\rm M_\odot pc}^{-2}$ for the SMGs, comparable to those in massive local ellipticals and Sa bulges. Similarly, Blain et al. (2004) provide tentative evidence for clustering of SMGs at a level consistent with the progenitors of $> L^*$ elliptical galaxies. These provide additional support for our conclusion that SMGs can be connected through a self-consistent evolutionary model to the local luminous galaxy population, which reproduces both the mass–luminosity relationship and luminosity distributions of local elliptical galaxies.

5 CONCLUSIONS

In this paper we have studied the rest-frame optical emission line structures and dynamics of six high redshift, luminous submm galaxies. Including two sources from the literature with similar observations, we find that of the eight submillimetre galaxies with resolved spectroscopy, at least five appear to comprise two or more dynamical sub-components. The average velocity offsets between these components is $\sim 180 {\rm km s}^{-1}$ across a projected spatial scale of 8 kpc. The obvious merging/interacting nature of these systems suggests there are analogous to the multi-component nature of the, typically less bolometrically luminous and slightly more compact, ULIRGs in the local Universe.

Since our IFU observations allow us to disentangle AGN and star-burst-like components (e.g. from [NII]/Hα flux ratios), it is perhaps significant that two of the eight submm galaxies shows possible signs of AGN activity in two spatially-resolved components on 1–2$''$ (10–20 kpc) scales.

Deep X-ray surveys of the *Chandra* Deep Field North have produced similar results: Alexander et al. (2003a) report that two of seven submm galaxies in this region are individually associated with pairs of X-ray sources on similar spatial scales (approximately one galactic diameter). Since the chance of a false association is $\lesssim 1\%$, it may be that we are witnessing the interaction or merging of AGNs in these sources (a low redshift example of this binary AGN activity is seen in the ULIRG NGC 6240; Komossa et al. 2003). The double AGN in some of these systems, suggests mergers may be responsible for disturbing the gas orbits in both components, hence fuelling subsequent AGN growth which currently lags behind a significant pre-existing stellar population (Alexander et al. 2003a; Smail et al. 2003).

By combining the spatially-resolved kinematic information from IFU, CO and longslit observations and assuming the velocity offsets we measure are eventually transformed into velocity dispersions in a pressure-supported galaxy, we derive dynamical masses of $5\pm3\times10^{11}$ $M_\odot$ for typical luminous submillimetre galaxies. This is similar to the dynamical masses found using Hα line widths (Swinbank et al. 2004) and resolved CO spectroscopy (Greve et al. 2005; Tacconi et al. 2006) and a factor of $\sim 2\times$ greater than the recent stellar mass estimates from Borys et al. (2005), suggesting that the central regions of these galaxies are baryon dominated.

We combine our dynamical measurement with estimates of the stellar luminosities for this population from Borys et al. (2005). We use these to constrain their likely evolution and so compare the properties expected for the descendents of submillimetre galaxies with $z = 0$ galaxy populations. We update the gas depletion time scales estimated by Greve et al. (2005) using recent results on the gas masses, bolometric luminosities and AGN contributions for this population, deriving typical gas depletion times of ~ 150 Myr. Adopting a typical burst duration of twice this age, ~ 300 Myr, we predict the evolution of their stellar populations and compare these to the Faber-Jackson relation for local ellipticals. For a ~ 300 Myr burst with a Kroupa IMF, we find that the expected fading would result in the descendents of the SMGs lying within ~ 0.2 mags of the FJ relation at their measured velocity dispersion. The same estimate of the lifetime can be used to correct the apparent space density of SMGs (assuming a galaxy only goes through one SMG phase in its lifetime) to derive a space density for the descendents of this population of $\sim 1.3 \times 10^{-4} \mathrm{Mpc}^{-3}$ for a population with $z = 0$ absolute luminosities of $M_K \sim -25.1$. Hence if SMGs have burst durations of ~ 300 Myr, as indicated by gas consumption timescales, then their predicted fading places them close to the present-day FJ relation. Moreover, the observed population at $z \sim 2$ is very comparable to that of luminous ellipticals with $M_K \lesssim -25.1$ ($\sim 3L_K^*$) at the present day.

Our observations show the power of using integral field spectroscopy around the rest-frame optical emission lines to probe the dynamics and power sources of these galaxies on $\gtrsim 5$ kpc scales. With forthcoming adaptive optics integral field spectroscopy on 8- and 10-m telescopes (e.g. OSIRIS on Keck, NIFS on Gemini and SINFONI on the VLT), we will soon be able to probe the dynamics, metallicities and star-formation properties on $\lesssim 0.1''$ (sub-kpc at $z = 2$) scales. Furthermore, the increased light grasp of large aperture telescopes will allow us to spatially resolve and map the absorption line spectra of these galaxies (including important diagnostic lines such as Ca II H&K, CH G-band, Hδ and MgB), allowing us to accurately probe the stellar contents and metallicity gradients, and so investigate the stellar ages and populations produced in these extreme systems. Such observations will allow us to probe further the timescales involved in the encounters as well as how and when these galaxies form most of their stars and thus the precise relation to similarly massive galaxies at the present day: luminous ellipticals.

REFERENCES

Alexander, D. M., Bauer, F. E., Brandt, W. N. Hornschemeier, A. E., Vignali, C., Garmire, G. P., Schneider, D. P., Chartas, G., & Gallagher, S. C. 2003a, AJ, 125, 383

Alexander, D. M., Bauer, F. E., Brandt, W. N., Schneider, D. P., Hornschemeier, A. E., Vignali, C., Barger, A. J., Broos, P. S., Cowie, L. L., Garmire, G. P., Townsley, L. K., Bautz, M. W., Chartas, G., & Sargent, W. L. W. 2003b, AJ, 126, 539

Alexander, D. M., Smail, I., Bauer, F. E., Chapman, S. C., Blain, A. W., Brandt, W. N., & Ivison, R. J. 2005, Nature, 434, 738

Almaini, O., Dunlop, J. S., Conselice, C. J., Targett, T. A., & Mclure, R. J. 2005, astro-ph/0511009

Alonso-Herrero, A., Ward, M. J., & Kotilainen, J. K. 1997, MNRAS, 288, 977

Baldwin, J. A., Phillips, M. M., & Terlevich, R. 1981, PASP, 93, 5

Baugh, C. M., Lacey, C. G., Frenk, C. S., Granato, G. L., Silva, L., Bressan, A., Benson, A. J., & Cole, S. 2005, MNRAS, 356, 1191

Bernardi, M., Sheth, R. K., Nichol, R. C., Schneider, D. P., & Brinkmann, J. 2005, AJ, 129, 61

Biggs, A., & Ivison, R. J. 2006, MNRAS submitted.

Blain, A. W., Chapman, S. C., Smail, I., & Ivison, R. 2004, ApJ, 611, 725

Blain, A. W., Jameson, A., Smail, I., Longair, M. S., Kneib, J.-P., & Ivison, R. J. 1999a, MNRAS, 309, 715

Blain, A. W., Smail, I., Ivison, R. J., & Kneib, J.-P. 1999b, MNRAS, 302, 632

Borys, C., Blain, A. W., Dey, A., Le Floc'h, E., Jannuzi, B. T., Barnard, V., Bian, C., Brodwin, M., Menéndez-Delmestre, K., Thompson, D., Brand, K., Brown, M. J. I., Dowell, C. D., Eisenhardt, P., Farrah, D., Frayer, D. T., Higdon, J., Higdon, S., Phillips, T., Soifer, B. T., Stern, D., & Weedman, D. 2006, ApJ, 636, 134

Borys, C., Smail, I., Chapman, S. C., Blain, A. W., & Ivison, R. J. 2006b, ApJ in prep.

Borys, C., Smail, I., Chapman, S. C., Blain, A. W., Alexander, D. M., & Ivison, R. J. 2005, ApJ, 635, 853

Bower, R. G., Morris, S. L., Bacon, R., Wilman, R. J., Sullivan, M., Chapman, S., Davies, R. L., de Zeeuw, P. T., & Emsellem, E. 2004, MNRAS, 351, 63

Cavanagh, B., Hirst, P., Jenness, T., Economou, F., Currie, M. J., Todd, S., & Ryder, S. D. 2003, in ASP Conf. Ser. 295: Astronomical Data Analysis Software and Systems XII, 237

Chapman, S. C., Smail, I. R., Blain, A. W., Ivison, R. J., & Swinbank, A. M. 2006, ApJ in prep.

Chapman, S. C., Blain, A. W., Ivison, R. J., & Smail, I. R. 2003a, Nature, 422, 695

Chapman, S. C., Blain, A. W., Smail, I., & Ivison, R. J. 2005, ApJ, 622, 772

Chapman, S. C., Smail, I., Windhorst, R., Muxlow, T., & Ivison, R. J. 2004, ApJ, 611, 732

Chapman, S. C., Windhorst, R., Odewahn, S., Yan, H., & Conselice, C. 2003b, ApJ, 599, 92

Croton, D. J., Farrar, G. R., Norberg, P., Colless, M., Peacock, J. A., Baldry, I. K., & Baugh et al. 2005, MNRAS, 356, 1155

Dasyra, K. M., Tacconi, L. J., Davies, R. I., Genzel, R., Lutz, D., Naab, T., Burkert, A., Veilleux, S., & Sanders, D. B. 2006, ApJ, 638, 745

Downes, D. & Solomon, P. M. 2003, ApJ, 582, 37

Faber, S. M. & Jackson, R. E. 1976, ApJ, 204, 668

Frayer, D. T., Armus, L., Scoville, N. Z., Blain, A. W., Reddy, N. A., Ivison, R. J., & Smail, I. 2003, AJ, 126, 73

Frayer, D. T., Ivison, R. J., Scoville, N. Z., Evans, A. S., Yun, M. S., Smail, I., Barger, A. J., Blain, A. W., & Kneib, J.-P. 1999, ApJL, 514, L13

Genzel, R., Baker, A. J., Tacconi, L. J., Lutz, D., Cox, P., Guilloteau, S., & Omont, A. 2003, ApJ, 584, 633

Greve, T. R., Bertoldi, F., Smail, I., Neri, R., Chapman, S. C., Blain, A. W., Ivison, R. J., Genzel, R., Omont, A., Cox, P., Tacconi, L., & Kneib, J.-P. 2005, MNRAS, 359, 1165

Greve, T. R., Ivison, R. J., Bertoldi, F., Stevens, J. A., Dunlop, J. S., Lutz, D., & Carilli, C. L. 2004, MNRAS, 354, 779

Hainline, L., Blain, A., Greve, T., Chapman, S. C., Smail, I. R., Ivison, 2006 MNRAS in prep.

Ivison, R. J., Greve, T. R., Smail, I., Dunlop, J. S., Roche, N. D., Scott, S. E., Page, M. J., Stevens, J. A., Almaini, O., Blain, A. W., Willott, C. J., Fox, M. J., Gilbank, D. G., Serjeant, S., & Hughes, D. H. 2002, MNRAS, 337, 1

Kennicutt, R. C. 1998, ARAA, 36, 189

Koekemoer, A. M., Fruchter, A. S., Hook, R. N., & Hack, W. 2002, in The 2002 HST Workshop : STSI, Baltimore, October 17-18, 2002. Ed. Arribas, Koekemoer & Whitmore. Baltimore, MD: STSI, 2002., p.339, 339

Komossa, S., Burwitz, V., Hasinger, G., Predehl, P., Kaastra, J. S., & Ikebe, Y. 2003, ApJL, 582, L15

Kovacs, A., Chapman, S. C., Dowell, C., Blain, A., Smail, Ivison, R. J., & Phillips, T.G., 2006, ApJ in press

Le Borgne, D., Rocca-Volmerange, B., Prugniel, P., Lançon, A., Fioc, M., & Soubiran, C. 2004, A&AP, 425, 881

Leitherer, C., Schaerer, D., Goldader, J. D., Delgado, R. M. G., Robert, C., Kune, D. F., de Mello, D. F., Devost, D., & Heckman, T. M. 1999, APJS, 123, 3

Lilly, S. J., Eales, S. A., Gear, W. K. P., Hammer, F., Le Fèvre, O., Crampton, D., Bond, J. R., & Dunne, L. 1999, ApJ, 518, 641

Łokas, E. L. & Mamon, G. A. 2001, MNRAS, 321, 155

Mamon, G. A. & Łokas, E. L. 2005, MNRAS, 363, 705

Manners, J. C., Johnson, O., Almaini, O., Willott, C. J., Gonzalez-Solares, E., Lawrence, A., Mann, R. G., Perez-Fournon, I., Dunlop, J. S., McMahon, R. G., Oliver, S. J., Rowan-Robinson, M., & Serjeant, S. 2003, MNRAS, 343, 293

Maraston, C. 1998, MNRAS, 300, 872

Maraston, C., Daddi, E., Renzini, A., Cimatti, A., Dickinson, C., Papovich, C., Pasquali, N., & Pirzkal, N. 2006, astro-ph/0604530

Mulchaey, J. S., Koratkar, A., Ward, M. J., Wilson, A. S., Whittle, M., Antonucci, R. R. J., Kinney, A. L., & Hurt, T. 1994, ApJ, 436, 586

Navarro, J. F., Frenk, C. S., & White, S. D. M. 1997, ApJ, 490, 493

Neri, R., Genzel, R., Ivison, R. J., Bertoldi, F., Blain, A. W., Chapman, S. C., Cox, P., Greve, T. R., Omont, A., & Frayer, D. T. 2003, ApJL, 597, L113

Pope, A., Borys, C., Scott, D., Conselice, C., Dickinson, M., & Mobasher, B. 2005, MNRAS, 358, 149

Romanowsky, A. J., Douglas, N. G., Arnaboldi, M., Kuijken, K., Merrifield, M. R., Napolitano, N. R., Capaccioli, M., & Freeman, K. C. 2003, Science, 301, 1696

Salpeter, E. E. 1955, ApJ, 121, 161

Scott, S. E., Fox, M. J., Dunlop, J. S., Serjeant, S., Peacock, J. A., Ivison, R. J., Oliver, S., Mann, R. G., Lawrence, A., Efstathiou, A., Rowan-Robinson, M., Hughes, D. H., Archibald, E. N., Blain, A., & Longair, M. 2002, MNRAS, 331, 817

Simpson, C. & Rawlings, S. 2000, MNRAS, 317, 1023

Smail, I., Chapman, S. C., Blain, A. W., & Ivison, R. J. 2004, ApJ, 616, 71

Smail, I., Chapman, S. C., Ivison, R. J., Blain, A. W., Takata, T., Heckman, T. M., Dunlop, J. S., & Sekiguchi, K. 2003, MNRAS, 342, 1185

Smail, I., Ivison, R. J., Blain, A. W., & Kneib, J.-P. 1998, ApJL, 507, L21

—. 2002, MNRAS, 331, 495

Swinbank, A. M., Smail, I., Bower, R. G., Borys, C., Chapman, S. C., Blain, A. W., Ivison, R. J., Howat, S. R., Keel, W. C., & Bunker, A. J. 2005, MNRAS, 359, 401

Swinbank, A. M., Smail, I., Chapman, S. C., Blain, A. W., Ivison, R. J., & Keel, W. C. 2004, ApJ, 617, 64

Tacconi, L. J., Genzel, R., Tecza, M., Gallimore, J. F., Downes, D., & Scoville, N. Z. 1999, ApJ, 524, 732

Tacconi, L. J., Neri, R., Chapman, S. C., Genzel, R., Smail, I., Ivison, R. J., Bertoldi, F., Blain, A., Cox, P., Greve, T., & Omont, A. 2006, ApJ, 640, 228

Takata, T., Sekiguchi, K., Chapman, S. C., Smail, I., Geach, J., Swinbank, A. M., Blain, A. W., & Ivison, R. J.

2006, ApJ in prep.

Tecza, M., Baker, A. J., Davies, R. I., Genzel, R., Lehnert, M. D., Eisenhauer, F., Lutz, D., Nesvadba, N., Seitz, S., Tacconi, L. J., Thatte, N. A., Abuter, R., & Bender, R. 2004, ApJL, 605, L109

Veilleux, S. & Osterbrock, D. E. 1987, APJS, 63, 295

Wake, D., 2006, MNRAS in prep.

Webb, T. M., Eales, S. A., Lilly, S. J., Clements, D. L., Dunne, L., Gear, W. K., Ivison, R. J., Flores, H., & Yun, M. 2003a, ApJ, 587, 41

Webb, T. M. A., Lilly, S. J., Clements, D. L., Eales, S., Yun, M., Brodwin, M., Dunne, L., & Gear, W. K. 2003b, ApJ, 597, 680

Wilman, R. J., Gerssen, J., Bower, R. G., Morris, S. L., Bacon, R., de Zeeuw, P. T., & Davies, R. L. 2005, Nature, 436, 227